Contact Areas of the Tibiotalar Joint

Gunther Windisch,[1] Boris Odehnal,[2] Reinhold Reimann,[1] Friedrich Anderhuber,[1] Hellmuth Stachel[2]

[1]Institute of Anatomy Graz, Medical University Graz, Austria, Harrachgasse 21, A 8010 Graz, Austria

[2]Institute of Discrete Mathematics and Geometry, Vienna University of Technology,
Wiedner Hauptstrasse 8-10/104/3, A 1040 Vienna, Austria

ABSTRACT: The contact areas between the articular surfaces of the talus and tibia are essential for understanding the mobility of the ankle joint. The purpose of our study was to reveal the contact area among the superior articular surface of the trochlea tali (target surface T) and the inferior articular surface of the tibia (query surface Q) under non–weight-bearing conditions in plantar flexion and dorsiflexion. Twenty cadaveric foot specimens were dissected and scanned by a three-dimensional (3D) laser scanner to obtain data point sets. These point sets were triangulated and a registration procedure performed to avoid any intersection of the two joint surfaces. For all points of the query surface Q, the closest distance to T was measured. In 11 of the 20 ankle joints, the contact area was larger in plantar flexion, in 5 it was nearly of equal size, and in 4 the two surfaces were found in a better congruence in dorsiflexion. The two articular surfaces can be in point or line contact and cause different motions while T is gliding on Q, so the original geometry of ligaments must be carefully reconstructed after injury or during total ankle replacement. © 2007 Orthopaedic Research Society. Published by Wiley Periodicals, Inc. J Orthop Res 25:1481–1487, 2007
Keywords: ankle joint; contact area; three-dimensional laser scanner; geometrical analyses

INTRODUCTION

The ankle joint plays a fundamental role in human locomotion. A number of investigators used different experimental approaches to reveal the functional anatomy of this joint.[1–5] An entire complex of normal behavior remains controversial; nevertheless, understanding motion remains the basis for treatment of joint degeneration, fractures, and ligament injuries. Given the unsatisfactory results of total ankle arthroplasty, the need exists for more accurate investigations.[6–9]

Many studies have attempted to clarify kinematics, patterns of ligament elongation, and the geometry of the articular surface. Only a few focused on the contact characteristics of the superior articular surface of the trochlea of the talus and the inferior articular surface of the tibia.[10–13] Patterns of contact areas between the trochlea and the tibia were investigated using accurate reconstruction and digitization of the relevant articular surfaces.

The aim of our study was to reveal the articular congruence and to measure distances between the inferior articular surface of the tibia (query surface Q) and the superior articular surface of the trochlea tali (target surface T) of non–weight-bearing human ankle joints. All data were generated by a laser scanner, and a mathematical model used to measure distances between the two articular surfaces in plantarflexion and dorsalflexion.

METHODS

Specimens Dissection

Twenty human cadaveric ankle joints were studied: 10 female (range, 61–96 years; median, 79) and 10 male (range, 36–94 years; median, 76), with combined mean ages of 77.5. Five left female, five right female, five left male, and five right male were dissected. All of them were embalmed to preserve the natural character of tissues and allow joint motion.[14] The joint capsule and medial and lateral ligaments were dissected, and the joint disarticulated.

Scanning Data via Three-Dimensional (3D) Laser Scanner

The superior articular surface of the trochlea of the talus and the inferior articular surface of the tibia were scanned separately using a Minolta Vivid-900 3D-Laser

Correspondence to: Gunther Windisch (Telephone: 43-316-380-7582; Fax: 43-316-380-69-7582;
E-mail: gunther.windisch@meduni-graz.at)
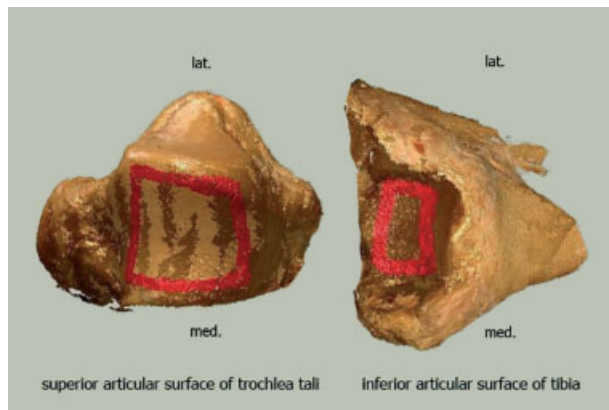
Figure 1. View from above of a right disarticulated ankle joint. The two scanned joint surfaces are marked in red. Abbreviations: lat, lateral side; med, medial side.

scanner to generate sets of 3D data (Fig. 1). Software [Polygon Editing Tool (PET), version 2.02] was used to assign coordinates to the data points.[15] For some objects, a single shot with the scanner and thus one 3D image is enough to create a digital model. For other objects, scans taken from two, three, or more different positions are useful. The scanner renders this feature through a turntable that can be controlled by the PET.

For a single shot, the data points need only to be triangulated to create a digital model. The triangulation procedure computes the edges and faces of a polyhedral model of the scanned surface. Thus it results in neighborhood relations between the data points and a list of those triplets that form triangular faces of the polyhedra (Fig. 2). Using multiple shots, two stages are necessary to obtain a 3D model: triangulation of each point set and alignment of single shots and creation of one object.

The second stage was more complicated and divided into four steps. The aim was to combine shots and rebuild the original object as follows: (1) a fixed part of the object was chosen and then (2) registration was performed by moving another part towards the fixed one. The main problem of standard registration methods is the absence of penetration control, so the moved and fixed object would in general intersect each other during the interactive process of registration and in the final
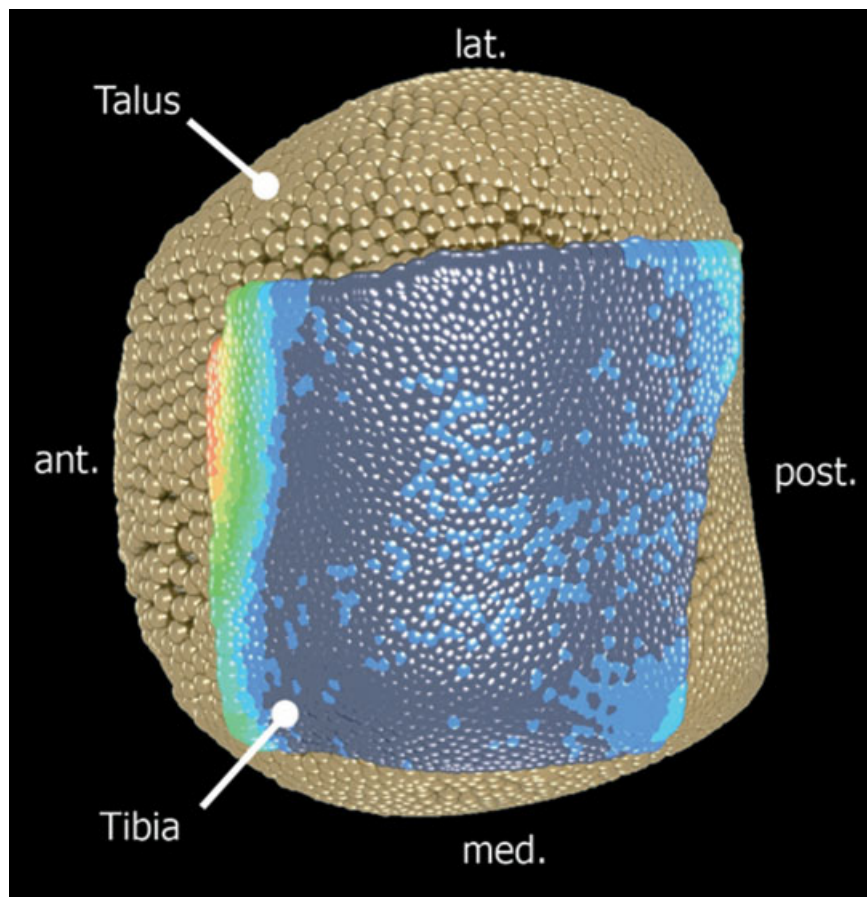
Figure 2. View from *inside* the tibia above *both* colored articular surfaces in plantar flexion. Dark blue spheres: nearest distance between the surfaces are congruent areas; red spheres: widest distance among the surfaces. The surrounding bone of the cartilaginous joint surface of the tibia was removed; some bony parts of the talus were left under the tibia to get an impression of the images after a scan.

position. The registration method we used is based on kinematics methods and the method of least squares.[16]

Overlapping of reassembled parts was a consequence of fact that subsequent shots with the scanner created images of overlapping regions of the object. The overlapping may cause inaccuracies in step four of the next two steps: (3) revision of the second step until all parts were reassembled and (4) retriangulation of the object. In this final step, the information of triangulations of different reassembled parts was removed, and the retriangulation created a new polyhedron. Folds of the new polyhedron were avoided by data smoothing. Smoothing removed spikes and outliers while preserving the overall shape of the surface.[17−20]

Registration without Penetration

The registration of the digitized surfaces was implemented such that intersections could not occur. Thus, we have not performed a pure minimization of the sum of squared distances; we also added punishing terms that accounted for intersections of surfaces (Fig. 3).

The registration was performed with (1) or without (2) correspondences. In case (1), the points of a list $[X_1,...,X_N]$ of points on the surface Q and the points of a list $[Y_1,...,Y_N]$ on the surface T, respectively, were known to correspond to each other. This means that after the registration we had $X_i = Y_i$ (for all indices $i \in \{1,...,N\}$). This was the ideal case; the surfaces were congruent and only differed from a rigid body motion. In case (2), we only looked for the best alignment of Q and T. Both methods used instantaneous kinematics of surfaces and local approximants of squared distances functions of surfaces.[16]

Comparison Algorithm

The most important part was to evaluate the deviation of the query Q surface from the target T surface. By simply computing the distances of all points in the query surface to all points in the target surface, we found the distribution of distances of the points in Q. The distances of a data point $P \in Q$ is defined as the minimum of the distances of P to any point in T. Thus, the comparison algorithm computed the nearest point $N \in T$ to P and the distance $||NP||$ is the distance of P to T. Doing this for all points in T, we obtained the function defined on Q that is displayed by means of a color map (see also Graphical Output section; Figs. 3, 4).

Implementation

For implementation, Matlab 7.5 was used on a PC with 2.4 GHz and 1 MB RAM.[21−23] The comparison algorithm applied to approximately 2000 points (which in fact was quite a small set in computational geometry) took at most 60 s, including preprocessing, that is, reading the data (consisting of the coordinates of the data points and the triangle list) and creating the list of vertex references.

Graphical Output

We wrote a routine to write data and results into a Povray-file (Povray is a free software, used to create photorealistic scenes with light models).[24] Data points were represented by spheres colored according to their distance to the target surface. Therefore, the minimal d_{min} and maximal d_{max} distances between the superior articular surface of the trochlea tali and the inferior articular surface of the tibia, the mean distance d_μ, and the standard deviation σ_d were determined.

Furthermore, the interval $\delta := d_{max} - d_{min}$ was divided into 10 intervals. Those points of the inferior articular surface of the tibia whose distances were in the interval I_1 $(d_{min}, d_{min} + \delta/10)$ were colored as dark blue spheres. With increasing distance, the points changed the color into blue, green, yellow, and finally
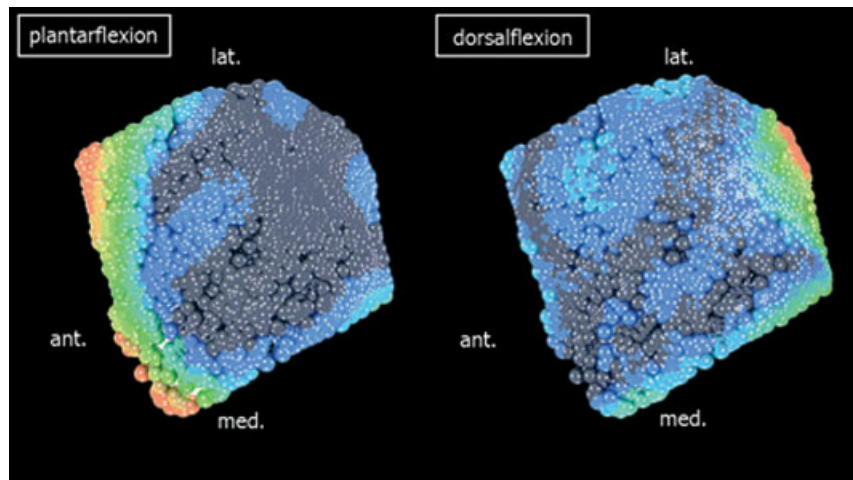
Figure 3. View from above on a right ankle joint; only the two joint surfaces are shown. There are many more dark blue spheres in plantar flexion; the joint surfaces are closer to each other, and the contact area is larger in this position.
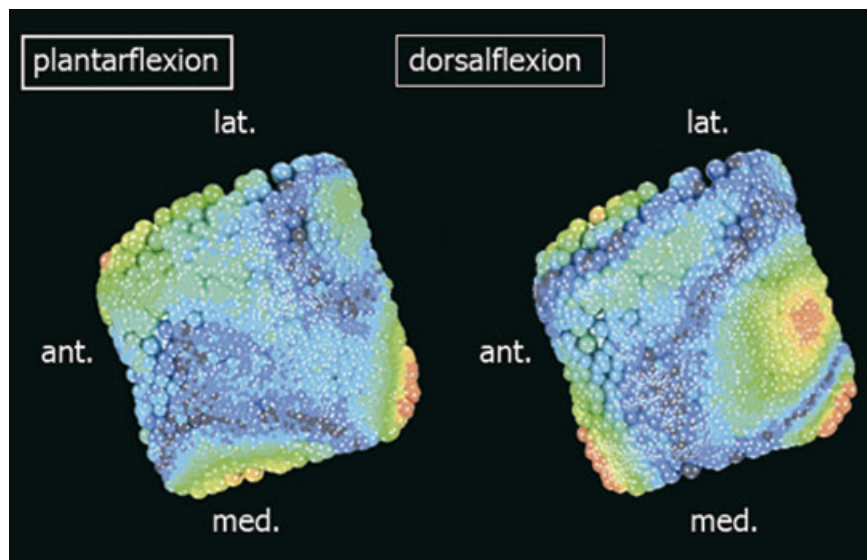
Figure 4. View from above on a right ankle joint. In a dorsiflexed position, the large distance in the mid-dorsal part of the joint surface is evident. [Color figure can be viewed in the online issue, which is available at www.interscience.wiley.com]

red for the greatest distance between the two joint surfaces (Figs. 3, 4).

RESULTS

The results showed that the contact area between the superior articular surface of the trochlea tali and the inferior articular surface of the tibia was greater in plantar flexion than in dorsiflexion (Tables 1–4). In 6 of 10 right specimens, the sum of I_1 and the I_2 was much higher in plantar flexion, so they were congruent in this position (Table 1, Fig. 3). In specimen f31_right, the maximal congruent contact area was found to be 84.8% in plantar flexion; in dorsiflexion, the data points came in 71.5% in close contact. In these six ankle

joints, the mean distance d_μ ranged in plantar flexion from 0.6 mm and 1.6 mm, and in dorsiflexion from 0.8 mm and 2.1 mm.

In two ankle joints (f06, f52), the contact areas were nearly the same in plantar flexion and dorsiflexion, whereas the contact was more congruent in dorsiflexion in two specimens (f02, f27). In these ankle joints, the mean contact area was 61.4% in plantar flexion and 69.80% in dorsiflexion (Table 3).

In 5 of 10 left ankle joints, the contact area was greater in plantar flexion; in specimen f07_left, a maximal congruent contact zones of 86.5% was reached in plantar flexion; in dorsalflexion only 63.7% were measured. The mean distance d_μ ranged from 0.5 mm to 1.1 mm in plantar flexion,

Table 1. Distances (in Millimeters) between the Two Joint Surfaces of the Right Ankle Specimens

Specimen		$d_{\min}$	$d_{\max}$	d_μ	σ_d	Specimen		$d_{\min}$	$d_{\max}$	d_μ	σ_d
f02_right	PF	0.07	13.98	3.33	3.91	f17_right	PF	0.03	7.90	1.56	1.54
	DF	0.02	6.76	0.63	0.75		DF	0.02	3.04	0.80	0.49
f05_right	PF	0.03	2.31	0.63	0.33	f27_right	PF	0.03	8.03	1.97	1.96
	DF	0.03	2.49	0.84	0.54		DF	0.04	12.92	2.01	2.41
f06_right	PF	0.02	9.46	1.41	1.60	f31_right	PF	0.05	6.89	0.98	1.06
	DF	0.03	4.58	0.58	0.45		DF	0.04	6.31	1.11	1.00
f09_right	PF	0.09	8.66	1.60	1.80	f52_right	PF	0.05	10.01	2.35	2.79
	DF	0.02	4.67	0.88	0.73		DF	0.04	9.12	1.48	1.46
f14_right	PF	0.04	7.11	1.39	1.19	f70_right	PF	0.05	8.11	1.42	1.60
	DF	0.02	8.76	2.12	2.20		DF	0.03	6.97	1.24	1.31

Abbreviations: PF, plantar flexion; DF, dorsiflexion; $d_{\min}$, minimal distance between articular surface of tibia and talus; $d_{\max}$, maximal distance between articular surface of tibia and talus; d_μ, mean distance among articular surface of tibia and talus; σ_d, standard deviation.

Table 2. Distances (in Millimeters) between the Two Joint Surfaces of the Left Ankle Specimens

Specimen		d_{min}	d_{max}	d_μ	σ_d	Specimen		d_{min}	d_{max}	d_μ	σ_d
f03_left	PF	0.06	7.62	1.48	1.72	f13_left	PF	0.06	8.51	1.10	1.32
	DF	0.03	4.83	0.63	0.08		DF	0.03	5.11	0.76	0.73
f07_left	PF	0.04	5.53	0.69	0.83	f14_left	PF	0.04	3.45	0.84	0.58
	DF	0.03	2.85	0.57	0.44		DF	0.05	5.14	0.80	0.67
f08_left	PF	0.01	0.35	0.55	0.37	f18_left	PF	0.03	5.31	1.09	1.06
	DF	0.02	6.05	0.91	0.93		DF	0.04	3.65	1.09	0.69
f11_left	PF	0.05	7.02	1.06	1.43	f27_left	PF	0.04	2.17	0.58	0.29
	DF	0.08	7.58	1.82	1.18		DF	0.04	11.20	1.24	1.69
f12_left	PF	0.05	2.64	0.51	0.30	f32_left	PF	0.05	1.99	0.61	0.34
	DF	0.04	4.23	0.58	0.50		DF	0.04	3.64	0.81	0.58

Abbreviations: PF, plantar flexion; DF, dorsiflexion; d_{min}, minimal distance between articular surface of tibia and talus; d_{max}, maximal distance between articular surface of tibia and talus; d_μ, mean distance among articular surface of tibia and talus; σ_d, standard deviation.

and in dorsiflexion a mean distance between 0.6 mm and 1.2 mm was found. Three specimens (f03, f11, f12) had nearly the same distribution of contact zones, and two articular surfaces were (f27, f32) more congruent in dorsiflexion. In these joints, the articular surfaces had a mean contact zone of 73.4% in dorsiflexion and 30.6% in plantar flexion (Table 4).

The contact area moved anteriorly with increased dorsiflexion and was much greater in the lateral part of the joint surfaces. The greatest distance between the query surface Q and the target surface T in all the cadaveric specimens was in the mid-dorsal part of the surfaces in a dorsiflexed position (Fig. 4).

DISCUSSION

Several attempts have been made to construct a geometrical model of the ankle joint complex. Reimann and colleagues studied the geometry of the trochlea tali and found that the lateral border, which had a screwed course, was bent round a fixed axis concentrically. The trochlea talus was characterized as a torus segment with an elliptical medial and a circular lateral main curve. A segment of a flat cone was added to this torus medially. On the lateral side, a segment of a screw body was amassed. Based on these data, a model was created, and pioneering model by Inman (the ankle as a single hinge joint) was disproved[25,26]:

Table 3. Intervals (%) of the Joint Surfaces of the Right Specimens

Specimen		I_1	I_2	I_3	I_4	I_5	I_6	I_7	I_8	I_9	I_{10}
f02_right	PF	58.48	4.50	4.45	5.36	4.45	3.54	5.08	3.64	6.37	3.13
	DF	58.11	13.03	3.21	1.77	0.86	1.25	0.43	0.29	0.34	0.71
f05_right	PF	5.71	26.21	31.29	16.25	10.74	4.16	2.66	1.79	0.77	0.44
	DF	6.72	24.42	20.55	15.91	6.91	5.90	6.04	5.56	4.30	3.68
f06_right	PF	53.28	25.84	4.90	4.21	4.21	2.57	1.65	1.19	1.01	1.15
	DF	44.85	40.77	10.40	1.28	0.69	0.46	0.46	0.46	0.32	0.32
f09_right	PF	51.57	23.21	5.09	3.51	2.91	3.46	3.36	2.37	2.27	2.07
	DF	23.90	46.37	12.40	7.60	2.86	1.63	1.48	1.43	0.94	1.38
f14_right	PF	33.43	29.84	14.44	8.75	4.40	3.20	2.82	1.10	1.10	0.91
	DF	46.05	14.20	6.55	6.55	5.45	4.78	4.64	4.35	3.68	3.73
f17_right	PF	41.15	25.73	9.19	7.11	4.20	3.70	3.42	2.54	1.66	1.29
	DF	7.90	30.85	26.65	15.70	7.02	4.11	3.51	2.12	1.15	0.97
f27_right	PF	38.10	21.73	10.28	5.84	4.68	3.96	3.77	3.67	3.86	4.10
	DF	55.87	18.64	7.29	5.46	3.72	2.51	2.32	1.83	1.21	1.16
f31_right	PF	50.24	34.56	5.13	2.64	1.37	1.47	1.12	1.08	1.03	1.37
	DF	37.73	33.77	12.22	5.23	2.79	2.79	2.74	1.27	0.98	0.49
f52_right	PF	51.80	15.40	3.60	2.73	3.65	3.79	4.65	4.17	4.17	6.04
	DF	42.54	27.15	16.16	5.71	2.30	1.63	1.44	0.82	0.86	1.39
f70_right	PF	53.46	21.67	5.20	4.01	2.63	3.15	4.68	2.82	1.48	0.91
	DF	47.73	25.20	9.31	3.77	2.96	3.39	2.43	2.24	1.77	1.19

Table 4. Intervals (%) of the Joint Surfaces of the Left Specimens

Specimen		I_1	I_2	I_3	I_4	I_5	I_6	I_7	I_8	I_9	I_{10}
f03_left	PF	46.36	28.33	6.66	3.15	2.53	2.00	2.09	2.31	2.22	4.35
	DF	61.32	24.11	4.48	2.49	1.95	1.60	1.64	0.84	0.85	0.75
f07_left	PF	66.01	20.54	4.06	2.23	1.70	1.34	1.30	0.94	0.80	1.07
	DF	19.56	44.17	20.54	5.94	2.95	1.88	1.38	1.43	0.94	1.21
f08_left	PF	12.78	36.90	24.39	9.03	5.47	4.20	3.48	2.35	1.26	0.14
	DF	50.09	28.14	7.59	4.47	3.16	2.08	1.67	0.99	0.68	0.86
f11_left	PF	71.88	7.64	3.49	2.93	3.28	3.01	2.75	1.66	1.14	2.23
	DF	44.24	34.85	7.73	4.50	2.71	1.40	1.35	1.22	0.79	1.22
f12_left	PF	18.07	42.23	26.51	7.10	2.53	2.00	0.65	0.26	0.26	0.39
	DF	39.66	47.50	5.75	2.79	1.09	0.78	0.70	0.61	0.44	0.70
f13_left	PF	60.20	23.89	5.41	2.92	2.81	1.39	1.05	1.09	0.74	1.13
	DF	46.03	33.26	9.11	4.49	2.27	1.13	1.35	1.00	0.65	0.70
f14_left	PF	12.55	36.66	25.61	7.84	4.71	4.43	3.50	2.75	1.21	0.75
	DF	35.96	44.92	7.60	3.12	3.08	2.57	1.26	5.70	0.33	0.47
f18_left	PF	28.87	38.96	15.01	3.35	1.97	2.29	2.80	2.07	1.47	2.94
	DF	7.89	22.21	26.11	19.92	8.54	4.18	3.53	2.07	2.48	3.07
f27_left	PF	6.55	25.33	31.42	21.19	7.32	2.96	2.96	1.55	0.59	0.14
	DF	73.90	11.19	6.55	1.73	1.50	1.32	1.00	0.91	0.82	1.09
f32_left	PF	5.77	23.61	28.43	19.84	7.94	4.08	3.17	3.56	2.56	1.04
	DF	15.23	46.48	13.45	8.16	5.51	4.04	3.99	2.56	0.26	0.30

during dorsiflexion, the trochlea is moved like a hinge, but during plantar flexion like a screw. These results were confirmed by Leardini and colleagues using stereophotogrammetric trials to define common reference coordinate systems under unloaded conditions.[11]

Many experimental studies have been reported contact areas, especially between the superior articular surface of the trochlea tali and the inferior articular surface of the tibia.[1,4,27–32] Only a few included mathematical models to collect data of contact areas between the tibia and talus and to make patterns of surface congruence in different joint positions.[10–12,33,34] Corazza and colleagues used roentgen stereophotogrammetric analysis and 3D digitization to create a model,[12] but they only evaluated three specimens, which were not marked consequently throughout the text and in the figures. The most important part for creating of a geometrical model was not mentioned in their study: penetration control after registration of digitized surfaces, which avoids intersections.

In our study, 20 ankle joints were scanned on a turntable to get data points from different positions. The advantage was the registration of the digitized surfaces that accounted for intersections of surfaces. It is the first time that the size of the contact areas between the superior articular surface of the trochlea tali and the inferior articular surface of the tibia were determined and the distances in between these joint surfaces measured.

In 6 of 10 right specimens and in 4 of 10 left ankles, the contact area was much greater in plantar flexion, reached a maximum congruence of 84.8% on the right and 86.6% on the left side. In a dorsiflexed position of the talus, a maximum of 74.5% on the right side and 85.1% on the left side was reached.

Although there were natural constraints for the best fit of the target and the query surface, no possibility existed to describe these constraints in a more mathematical way. The geometric type of contact between the two surfaces Q and T remains unknown. The local surface shapes could be part of a helical surface as observed previously.[10,11,25] Helical surfaces can be in point or line contact. Both contact types cause different motions, while T is gliding along Q: during plantar/dorsiflexion, medial–lateral as well as anteroposterior translations occur. Careful reconstruction of the original geometry of ligaments is absolutely necessary after injury or during total ankle replacement.[10,11]

REFERENCES

1. Ramsey PL, Hamilton W. 1976. Changes in tibiotalar area of contact caused by lateral talar shift. J Bone Joint Surg [Am] 58:356–357.
2. Kimizuka M, Kurosawa H, Fukubayashi T. 1980. Load-bearing pattern of the ankle joint. Contact area and pressure distribution. Arch Orthop Trauma Surg 96: 45–49.

3. Macko VW, Matthews LS, Zwirkoski P, et al. 1991. The joint- contact area of the ankle. The contribution of the posterior malleolus. J Bone Joint Surg [Am] 73:347–351.

4. Pereira DS, Koval KJ, Resnick RB, et al. 1996. Tibiotalar contact area and pressure distribution: the effect of mortise widening and syndesmosis fixation. Foot Ankle Int 17: 269–274.

5. Michelson JD, Checcone M, Kuhn T, et al. 2001. Intraarticular load distribution in the human ankle joint during motion. Foot Ankle Int 22:226–233.

6. Bentley G, Shearer J. 1996. The foot and ankle. In: Duthie RB, Bentley G, editors. Mercer's orthopaedic surgery. Paris: Arnold; p 1193–1253.

7. Kitaoka H, Patzer G. 1996. Clinical results of the Mayo total ankle arthrosplasty. J Bone Joint Surg [Am] 78: 1658–1664.

8. Lachiewicz P. 1994. Total ankle arthroplasty: indications, techniques and results. Orthop Rev 23:315–320.

9. Lewis G. 1994. the ankle joint prosthetic replacement: clinical performance and research challenges. Foot Ankle Int 15:471–476.

10. Leardini A, O'Connor JJ, Catani F et al. 1999. A geometric model of the human ankle joint. J Biomech 32:585–591.

11. Leardini A, O'Connor JJ, Catani F, et al. 1999. Kinematics of the human ankle complex in passive flexion; a single degree of freedom system. J Biomech 32:111–118.

12. Corazza F, Stagni R, Castelli VP, et al. 2005. Articular contact at the tibiotalar joint in passive flexion. J Biomech 38:1205–1212.

13. Siegler S, Chen J, Schneck C. 1988. The three- dimensional kinematics and flexibility characteristics of the human ankle and subtalar joints. Part 1: kinematics. J Biomech Eng 110:364–373.

14. Thiel W. 1992. Die Konservierung ganzer Leichen in natürlichen Farben. [The preservation of the whole corps with natural color]. Ann Anat 174:185–195.

15. The polygon editing tool. Available from http://www.konicaminolta-ed.com.

16. Pottmann H, Leopoldseder S, Hofer M. 2004. Registration without ICP. Comput Vis Image Understanding 95: 54–71.

17. Hoschek J, Lasser D. 1993. Fundamentals of CAGD Wellesley, MA: Peters; 1993.

18. Haussmann W. 2002. Modern developments in multivariate approximation. Paper presented at: Fifth International Conference. Germany.

19. Stollnitz EJ, DeRose T, Salesin DH. 1996. Wavelets for computer graphics San Francisco: Morgan Kaufmann.

20. Warren J. 2001. Subdivision methods for geometric design San Francisco: Morgan Kaufmann.

21. Matlab. Available from http://www.mathworks.com/products/matlab.

22. Otto S, Denier JP. 2005. An introduction to programming and numerical methods London: Springer.

23. Hanselmann CD, Littlefield BL. 2004. Mastering Matlab 7. Englewood Cliffs, NJ: Prentice Hall.

24. Povray: the persistance of vision ray tracer. Available from: http://www.povray.org.

25. Reimann R, Anderhuber F, Gerold J. 1986. Über die Geometrie der menschlichen Sprungbeinrolle. Acta Anat 127:271–278.

26. Inmann VT. 1976. The joints of the ankle Baltimore: Williams and Wilkins.

27. Bertsch C, Rosenbaum D, Claes L. 2001. Intra-articular and plantar pressure distribution of the ankle joint complex in relation to foot position. Unfallchirurg 104: 426–433.

28. Clarke HJ, Michelson JD, Cox QG, et al. 1991. Tibiotalar stability in bimalleolar ankle fractures: a dynamic in vitro contact area study. Foot Ankle Int 11:222–227.

29. Curtis MJ, Michelson JD, Urquhart MW, et al. 1992. Tibiotalar contact and fibular malunion in ankle fractures. A cadaver study. Acta Orthop 63:326–329.

30. Driscoll HL, Christensen JC, Tencer AF. 1994. Contact characteristics of the ankle joint. J Am Podiat Med Assn 84:491–498.

31. Earll M, Wayne J, Brodrick C, et al. 1996. Contribution of the deltoid ligament to ankle joint contact characteristics: a cadaver study. Foot Ankle Int 17:317–324.

32. Hartford JM, Goczyca JT, McNamara JL, et al. 1995. Tibiotalar contact area. Clin Orthop 320:182–187.

33. Siegler S, Udupa JK, Ringleb SI, et al. 2005. Mechanics of the ankle and subtalar joints revealed through a 3D quasi-static sttress MRI technique. J Biomech 38:567–578.

34. Lundberg A, Svensson O, Nemeth G, et al. 1989. The axes of rotation of the ankle joint. J Bone Joint Surg [Br] 71: 481–495.